Journal of Power Sources 195 (2010) 4143–4148

Contents lists available at ScienceDirect

Journal of Power Sources

journal homepage: www.elsevier.com/locate/jpowsour

Quantitative characterization of water transport and flooding in the diffusion layers of polymer electrolyte fuel cells

A. Casalegno*, L. Colombo, S. Galbiati, R. Marchesi

Department of Energy, Politecnico di Milano, via Lambruschini 4, 20156 Milano, Italy

ARTICLE INFO

Article history:
Received 7 August 2009
Received in revised form
17 November 2009
Accepted 17 January 2010
Available online 25 January 2010

Keywords:
Fuel cell
PEFC
Water transport
Experiment
Flooding
Diffusion layer

ABSTRACT

Optimization of water management in polymer electrolyte membrane fuel cells (PEMFC) and in direct methanol fuel cells (DMFC) is a very important factor for the achievement of high performances and long lifetime. A good hydration of the electrolyte membrane is essential for high proton conductivity; on the contrary water in excess may lead to electrode flooding and severe reduction in performances. Many studies on water transport across the gas diffusion layer (GDL) have been carried out to improve these components; anyway efforts in this field are affected by lack of effective experimental methods. The present work reports an experimental investigation with the purpose to determine the global coefficient of water transport across different diffusion layers under real operating conditions. An appropriate and accurate experimental apparatus has been designed and built to test the single GDL under a wide range of operating conditions. Data analysis has allowed quantification of both the water vapor transport across different diffusion layers, and the effects of micro-porous layers; furthermore flooding onset and its consequences on the mass transport coefficient have been characterized by means of suitably defined parameters.

© 2010 Elsevier B.V. All rights reserved.

1. Introduction

Polymer electrolyte membrane fuel cells (PEMFC) are still affected by technological issues limiting their performances and duration. One of the most investigated problems in experimental research is water management: a good hydration of polymer electrolyte membrane is essential to keep high its proton conductivity; on the other side excess of water may cause flooding of gas diffusion layers (GDL) and electrodes with a sensible decrease in efficiency. Membrane dehydration and electrode flooding, due to incorrect water management, have a dramatic effect on both performance and lifetime [1,2]. Moreover, water management is complicated by variable load operation, typical of real PEMFC applications, that determines variable water production and operating conditions. Thus during transients both dehydration and flooding could easily occur. Water transport in PEMFC origins from the complex combination of diffusive, convective and electro-osmotic phenomena with phase change and local water production, strongly influenced by the GDL characteristics [3]. Moreover, it is acknowledged that the interposition of a micro-porous layer (MPL) between the GDL and the catalyst layer greatly reduces flooding effect and improves fuel cell performance; however, the explanation for this improvement is still a subject for debate [4–6].

For this reason humidification of reactant flows has to be optimized in considering water transport properties of the gas diffusion layer. In the current literature these properties have been partially investigated, but neither general methods nor large amount of data under real operating conditions are still available. In particular, the lack of experimental results limits the knowledge about water management in PEMFC, which plays an essential role for the development of this technology, as already stated.

Several experimental investigations on water transport through GDL have been carried out with the purpose to improve water management in PEMFC [2,3].

Some of them make use of imaging techniques for studying water dynamics and distribution inside fuel cells, including direct visualization [7], neutron imaging [8], magnetic resonance imaging [9] and X-ray imaging [10]. Few of them test GDL singularly in order to characterize water transport and flooding effect, but operating conditions are generally different from real applications [11–14]. The greater part evaluates the effect of GDL properties on flooding by characterization of different physical indicators [15–22] during the operation of a complete fuel cell, but the presence of different phenomena and various components makes the interpretation of results difficult.

The development of a methodology to characterize quantitatively and in real operating conditions water transport and flooding in GDL could allow:

* Corresponding author. Tel.: +39 0223993912; fax: +39 0223993863.
E-mail address: andrea.casalegno@polimi.it (A. Casalegno).

0378-7753/$ – see front matter © 2010 Elsevier B.V. All rights reserved.
doi:10.1016/j.jpowsour.2010.01.032

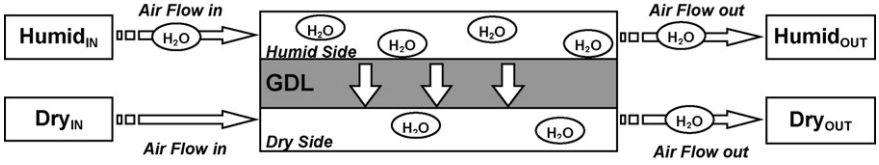

Fig. 1. Simplified scheme of the testing apparatus.

- to increase the understanding of these phenomena and their impact on reactant transport and fuel cell operation;
- to optimize accurately GDL and MPL properties;
- to validate models in order to contribute both to a deeper understanding of transport phenomena in porous materials and to optimize fuel cell control systems for longer lifetime.

A contribution in this direction is the aim of the present work. To perform quantitative characterization of water transfer across a gas diffusion layer subject to real operating conditions, a dedicated experimental apparatus has been realized. Tests have been carried out in order to obtain a complete description of water transport; furthermore flooding conditions have been observed and investigated as well. The developed experimental procedure can be standardized for systematic characterization of GDL.

2. Methodology

2.1. Experimental approach

The experimental method consists in supplying GDL faces with a humid air flow and a dry air flow, respectively, in a co-current configuration, as represented in the simplified scheme reported in Fig. 1. In these conditions water transfer takes place across the porous medium from the humid side to the dry one.

Pressure differences between the two air flows across the GDL are suitably minimized, consequently permeation phenomena through the GDL can be neglected and water concentration difference becomes the main cause of mass transfer, determining a predominant diffusive mechanism. During the process, the water content decreases in the humid air flow, while it increases in the dry air flow, thus the outlet concentrations may be very close; nevertheless, for sake of simplicity, in the present work the flows and their channels will be named "dry" (D) and "humid" (H), respectively, with reference to the inlet conditions.

The system can be described by the following set of equations in which V indicates volumetric flow, C concentration. All the gases, and also water vapor, are supposed to have an ideal behavior; moreover, air is considered as a single chemical specie, keeping the molar ratio between nitrogen and oxygen constant.

- Air conservation equation

$$V_{\mathrm{H}}^{in} \cdot C_{air}^{\mathrm{H},in} + V_{\mathrm{D}}^{in} \cdot C_{air}^{\mathrm{D},in} = V_{\mathrm{H}}^{out} \cdot C_{air}^{\mathrm{H},out} + V_{\mathrm{D}}^{out} \cdot C_{air}^{\mathrm{D},out} \quad (1)$$

- Water conservation equation

$$V_{\mathrm{H}}^{in} \cdot C_{\mathrm{H_2O}}^{\mathrm{H},in} + V_{\mathrm{D}}^{in} \cdot C_{\mathrm{H_2O}}^{\mathrm{D},in} = V_{\mathrm{H}}^{out} \cdot C_{\mathrm{H_2O}}^{\mathrm{H},out} + V_{\mathrm{D}}^{out} \cdot C_{\mathrm{H_2O}}^{\mathrm{D},out} \quad (2)$$

- State equation at humid inlet

$$C_{\mathrm{H_2O}}^{\mathrm{H},in} + C_{air}^{\mathrm{H},in} = \frac{P_{\mathrm{H}}^{in}}{RT_{\mathrm{H}}^{in}} \quad (3)$$

- State equation at dry inlet

$$C_{\mathrm{H_2O}}^{\mathrm{D},in} + C_{air}^{\mathrm{D},in} = \frac{P_{\mathrm{D}}^{in}}{RT_{\mathrm{D}}^{in}} \quad (4)$$

- State equation at humid outlet

$$C_{\mathrm{H_2O}}^{\mathrm{H},out} + C_{air}^{\mathrm{H},out} = \frac{P_{\mathrm{H}}^{out}}{RT_{\mathrm{H}}^{out}} \quad (5)$$

- State equation at dry outlet

$$C_{\mathrm{H_2O}}^{\mathrm{D},out} + C_{air}^{\mathrm{D},out} = \frac{P_{\mathrm{D}}^{out}}{RT_{\mathrm{D}}^{out}} \quad (6)$$

The previous set consists in 6 equations with 20 variables and results undetermined; the measurement of 14 physical parameters is thus necessary to solve it. The measured quantities are pressure, temperature, relative humidity and molar air flow at both inlets and at the dry outlet. At the humid outlet only pressure and temperature measurements are required to complete the system description, nevertheless, the relative humidity at humid outlet is also measured to verify mass conservation.

The water flow through the GDL can be calculated as:

$$\dot{N}_{\mathrm{GDL}} = V_{\mathrm{D}}^{out} \cdot C_{\mathrm{H_2O}}^{\mathrm{D},out} - V_{\mathrm{D}}^{in} \cdot C_{\mathrm{H_2O}}^{\mathrm{D},in} \quad (7)$$

This allows carrying out a complete characterization of GDL properties, giving useful indications for material optimization. During the experimental activity, particular care has been dedicated to the observation of flooding, in terms of both the onset conditions and the influence on PEMFC performances.

2.2. Experimental setup

A scheme of the experimental setup is reported in Fig. 2. The gas diffusion layer (surface area exposed to fluxes: 42 mm × 42 mm) is contained between two graphite distributors, where channels for humid and dry air flows have been grooved (both distributors have a triple serpentine channel with a square section: depth 0.8 mm, width 0.8 mm, length 700 mm). Graphite distributors are held together with two stainless steel plates using 8 retaining bolts closed with a controlled torque of 13 (±0.5) Nm applied with a certified instrument. A slot in one of the steel plates accommodates a calibrated thermocouple (uncertainty 0.1 K), connected with both a temperature controller and a data acquisition system. Two electrical heaters, connected to the temperature controller, are placed within the steel plates, to fully control the temperature of the assembly. Since heat capacity of the plates is much greater in comparison with those of graphite distributors and GDL, high temperature stability is attained. Furthermore, GDL thickness is generally very small (approximately 400 μm), hence thermal equilibrium with plates and distributors can be assumed. The rates of the air flows, supplied by a compressor, are controlled and measured by two calibrated flow controllers (maximum flow rate: 2 Nl min^{-1}; uncertainty: 0.7% + 0.004 Nl min^{-1}). Humidification is obtained by adding bidistilled water to the air stream by means of a peristaltic pump (water flow range: 3–100 g h^{-1}, uncertainty: 1%). Fluid flows are then heated in two different heat exchangers, consisting of stainless steel tubes (internal diameter: 10 mm, external diameter: 12 mm) with adhesive thermal resistances applied along the whole external surface. The heat exchanger on the humid side works as an evaporator, since it receives a two-phase flow (air and liquid water) and produces a homogeneous air and vapor mixture.

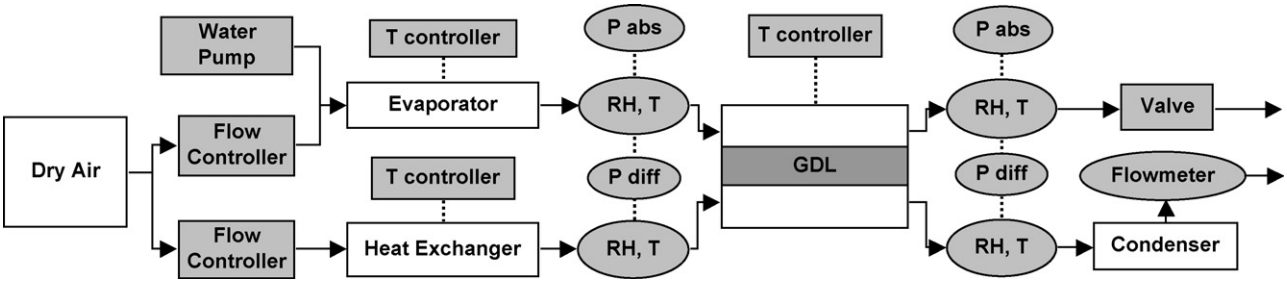

Fig. 2. Experimental setup scheme; grey squares represent controlled parameters, while grey rounds represent measured parameters.

Temperatures are measured on the external surface at the outlet section by two calibrated thermocouples (uncertainty 0.2 K) connected with two temperature controllers. These devices modulate the activity of adhesive resistances to keep temperature constant at a set-point value. Absolute pressures are measured at humid inlet and at dry outlet by two pressure transducers (pressure range: 0–3 bar, uncertainty: 2 mbar). Two differential pressure transducers are also used to measure pressure differences between the air flows at GDL inlet (range: 0–350 mbar, uncertainty: 0.2 mbar) and outlet (range: 0–500 mbar, uncertainty: 0.5 mbar). Absolute pressures at dry inlet and at humid outlet are thus obtained as the sum of the measured absolute and differential pressures. Pressure difference between the two flows at GDL inlet is minimized controlling mass flow rates by the two flow controllers; pressure difference between flows at GDL outlet is minimized regulating a precision valve situated at humid outlet. Relative humidity measurements are carried out at GDL inlets and outlets on both flows with four certified temperature and humidity transmitters based on a capacitive sensor (temperature range: 0–120 °C, uncertainty: 0.3 °C; humidity range 0–100%, uncertainty (over 40 °C): 1.5% + 1.5% of RH measure). The water present in the air flow at the dry outlet is condensed and separated with a "tube in tube" condenser, cooled with a water stream at approximately 15 °C; the outgoing molar air flow is measured by a calibrated flow meter (uncertainty: 0.7% + 0.004 Nl min^{-1}) and the residual water content is calculated from the measured temperature, generally lying between 25 and 30 °C, considering saturated air. Plant components are connected by thermally insulated PTFE tubes (outer diameter: 1/8 in.) with minimal length in order to reduce thermal losses, while connections are made through stainless steel fittings.

2.3. Data processing

All the measured parameters (pressures, flow rates, temperatures and relative humidities) have been acquired at 1 Hz frequency for 1500s in steady state conditions. Data have been processed with a robust method for outliers elimination[1]. Representative values of each parameter have been obtained as the average of the first 1000 elements among the remaining ones.

The measured quantities allow solving the system of equation described in the previous section, in particular by calculation of water concentrations and volumetric flows.

Water concentrations at GDL inlets and outlets can be obtained, according to the hypothesis of ideal air–vapor mixture, as:

$$C_{H_2O} = \frac{P_{H_2O}}{RT} = \frac{RH \cdot P^{sat}_{H_2O}}{RT} \tag{8}$$

where P_{H_2O} is the partial vapor pressure, that results from the product of relative humidity (RH) and vapor saturation pressure at flow temperature ($P^{sat}_{H_2O}$), R is the universal gas constant and T is the flow absolute temperature.

Similarly, volumetric flows at GDL inlets and outlets can be calculated as:

$$V = \frac{\dot{N}_{air}}{C_{air}} \tag{9}$$

2.4. Uncertainty, reproducibility and reliability analyses

Uncertainty was evaluated for both water concentrations and water flow through the GDL. It was estimated by combining uncertainties of the different instruments as indicated in [23] in order to obtain the global uncertainty of the experimental plant. Estimated values are 4% for water concentration and 7% for water flow through the GDL. The uncertainty analysis evidences that these values are approximately constant in the whole range of operating conditions investigated during the experimental campaign.

Results reproducibility was verified by repeating every single experimental measure in three different days. Water transport results were compared by ANOVA [23]. This analysis confirmed that differences between the days are not statistically significant, compared to measurement uncertainty, thus the experimental results are reproducible.

As already stated, relative humidity at humid outlet is measured to verify mass conservation. In the investigated conditions the difference between inlet and outlet water flows is generally 5%, less than measurement uncertainty.

Generally the pressure control system permits to reduce pressure differences between the two flows to approximately 1 mbar at both GDL inlet and outlet. The effect of this pressure difference across the GDL on water transport was investigated: some measurements were carried out with higher pressure difference between the two inlet flows (approximately 7 mbar). The results were compared with the values obtained during standard measurements at the same operating conditions. The variation of water flow through the GDL caused by such a pressure difference resulted below 4%, less than measurement uncertainty. Thus, the typical value of 1 mbar determines a water flow variation lower than 1%, negligible compared to uncertainty. These results confirmed that the developed pressure control system allows to make water transfer due to permeation negligible.

3. Results and discussion

As previously pointed out, the main goal of the experimental campaign is the description of the water transfer across the GDL and, more specifically, the characterization of flooding, that is the onset of condensation within the pores. Three different GDL, with and without MPL, have been considered, in order to put in evidence peculiar behaviors, Table 1. Thus, in the following, presentation and comparison of the experimental results will be followed by a discussion aimed to physical interpretation,

[1] The method eliminates values not included in the interval median ±3 times standard deviation, estimated through median absolute deviation (MAD).

Table 1
Characteristic of investigated gas diffusion layers.

	Thickness (μm)	PTFE content (%)	MPL
SGL10CC	410	10	Yes
SGL10AC	380	10	No
ELAT LT1400W	400	n.d.	Yes

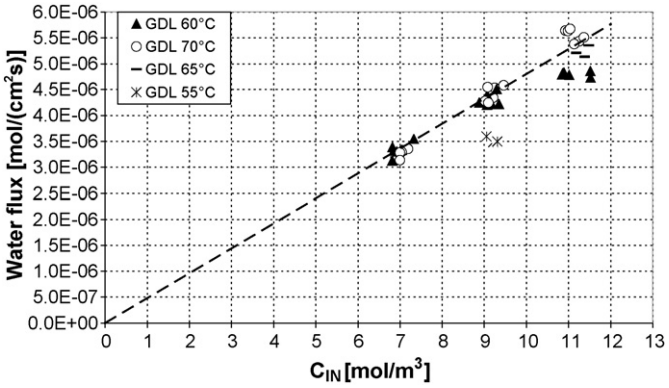

Fig. 3. Water molar flux versus inlet concentration.

together with the attempt to define a synthetic index of flooding onset.

The GDL SGL10CC with micro-porous layer (see Table 1) is considered at first. In Fig. 3 the water molar flux is reported versus water concentration at humid inlet for a wide range of GDL temperatures (55–70 °C). Repeated data series are plotted separately to point out the good reproducibility of measurements, already discussed in previous section. It is evident that most of the data are aligned along a straight line, as expected, with a few relevant exceptions: actually, measures relative to the lower values of GDL temperature (namely, 55 and 60 °C), lie down[2]. This means that a reduction in the water flux at the same inlet concentration is observed at these operating conditions, where the low GDL temperature gives rise to flooding.

To carry out a more detailed analysis, a global water transfer coefficient can be defined, assuming that the mass flow can be expressed as follows:

$$\dot{N}_{GDL} = K \cdot A \cdot \Delta C_{lm} \tag{10}$$

where $\dot{N}_{GDL}$ is the water flux across the GDL [mol s^{-1}]; A is the mass exchange surface [cm^2]; K is the global water transport coefficient[3] [cm s^{-1}]; ΔC_{lm} is the logarithmic mean difference of vapor concentration across the GDL [mol cm^{-3}], defined as:

$$\Delta C_{lm} = \frac{(C^{H,in}_{H_2O} - C^{D,in}_{H_2O}) - (C^{H,out}_{H_2O} - C^{D,out}_{H_2O})}{\ln \frac{(C^{H,in}_{H_2O} - C^{D,in}_{H_2O})}{(C^{H,out}_{H_2O} - C^{D,out}_{H_2O})}} \tag{11}$$

Interesting representations can be obtained by plotting both the water flux $\dot{N}_{GDL}/A$ and K versus ΔC_{lm}, as reported in Figs. 4 and 5, respectively.

The first drawing is quite similar to Fig. 3, but here the flooding onset is put in evidence by both a reduction in the mass flux and an increase in the mean water concentration difference between the streams. In this respect it is worth noting that, in contrast with the

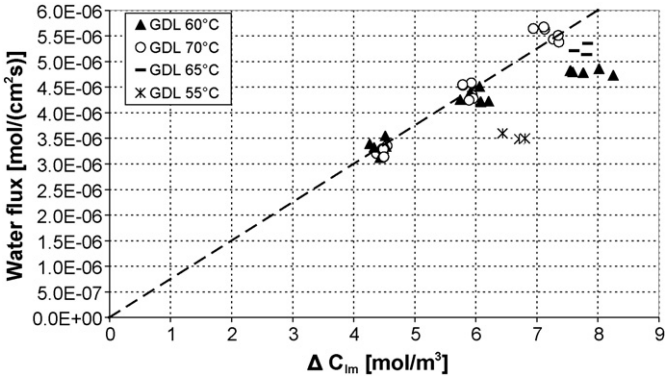

Fig. 4. Water molar flux versus logarithmic mean concentration.

representation of Fig. 3, also the data series corresponding to 65 °C GDL temperature seems to indicate that flooding occurs, although fairly, at this operating condition.

The same indication is provided by Fig. 5, where for all the mentioned data series a progressive reduction in the global water transfer coefficient is observed as the GDL temperature decreases and the water inlet concentration increases.

It should be noted, however, that the definition of ΔC_{lm} given above could lead to an underestimation of the global water transport coefficient. Actually, in a large number of experimental conditions heat transfer might occur in the entrance region of the humid channel, where mass exchange does not take place yet. The related cooling could increase relative humidity toward saturation, thus water condensation might occur at the channel walls. Unfortunately, it is impossible to determine the exact value of the water concentration at the inlet of the region where both heat and mass transfer occur together. Nevertheless, if condensation takes place, the mean concentration difference has a minimum value, corresponding to an inlet water concentration $C^{H,in}_{H_2O} = C^{sat}_{H_2O}$, given by:

$$\Delta C_{lm,2} = \frac{(C^{sat}_{H_2O} - C^{D,in}_{H_2O}) - (C^{H,out}_{H_2O} - C^{D,out}_{H_2O})}{\ln \frac{(C^{sat}_{H_2O} - C^{D,in}_{H_2O})}{(C^{H,out}_{H_2O} - C^{D,out}_{H_2O})}} \tag{12}$$

Consequently, the use of $\Delta C_{lm,2}$ instead of ΔC_{lm} in Eq. (10) leads to an overestimation of K.

It is interesting to compare the results obtained in this case for the water flux, reported in Fig. 6 with those depicted in Fig. 4. Data appear linearly correlated with the mean concentration difference and, in contrast with Fig. 4, they do not suggest relevant variations in the global water transfer coefficient. Only slight deviations

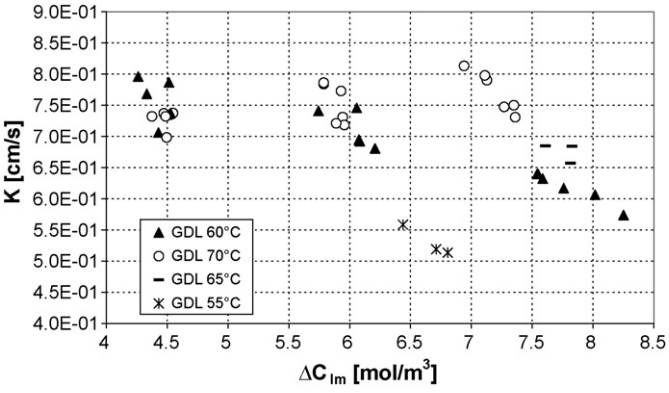

Fig. 5. Global water transfer coefficient versus logarithmic mean concentration.

[2] At 55 °C water concentration higher than 9.5 mol m^{-3} is not allowed by the present experimental setup because of condensate presence at humid outlet, that invalidates relative humidity measurement.

[3] Measurement uncertainty for the global water transport coefficient K has been estimated equal to 8%.

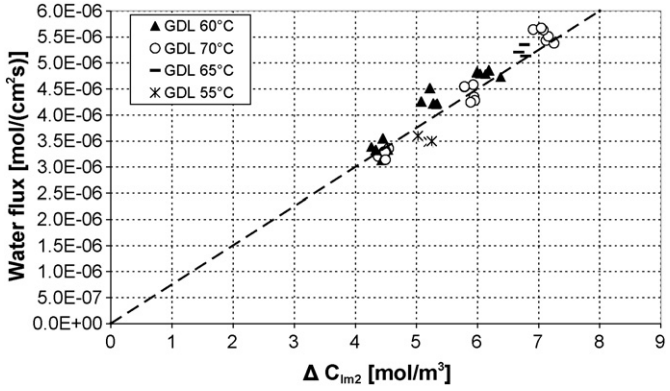

Fig. 6. Water molar flux versus logarithmic mean concentration.

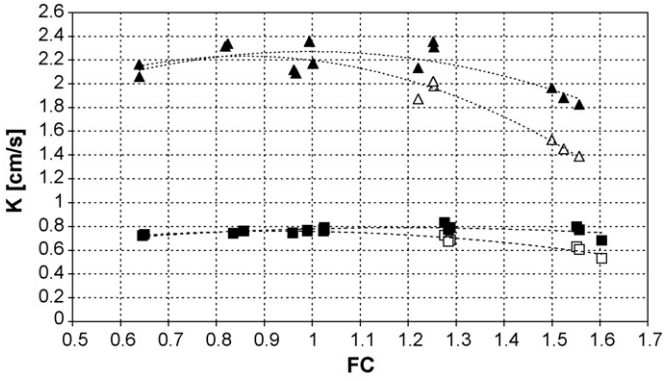

Fig. 8. Global water transfer coefficient versus flooding index for SGL10CC (squares) and SGL10AC (triangles).

are observed: in particular, the water flux results a little lower at the lowest GDL temperature, thus indicating the flooding onset, as already observed. However, the higher value of the mass flux for the same mean concentration difference at 60 °C GDL temperature (black triangles) cannot be easily interpreted and could be only a consequence of the mentioned overestimation of the global water transfer coefficient.

Based on the previous considerations, it is expected that flooding occurs if the following index, named flooding coefficient (FC), is higher than 1:

$$FC = \frac{C_{H_2O}^{H,in}}{C_{H_2O}^{sat}} > 1 \tag{13}$$

In Fig. 7 the global water transfer coefficient is reported as a function of FC for all the operative conditions. The two data series refer to the different evaluation of ΔC_{lm} in Eq. (10), as previously discussed: the real value of K will be bounded in the region between the fitting curves. It is to be noted that for $FC < 1$ both the curves are practically overlapping and any significant variation of the global water transfer coefficient is not observed. On the contrary, a reduction of K may be observed for $FC > 1$ due to flooding and it seems to become more relevant for $FC > 1.3$. The maximum expected reduction of K is about 20% with FC equal to 1.6. This is in good agreement with data reported in literature about performance decay due to flooding [3,17–22].

To compare the presented data with some available models, a two-layer structure composed by MPL and GDL has been considered. The known geometrical characteristics are listed in Table 2 together with model predictions.

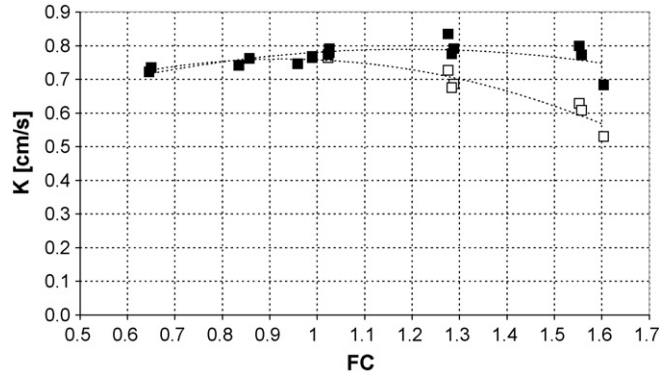

Fig. 7. Global water transfer coefficient versus flooding index, considering ΔC_{lm} (white squares) and $\Delta C_{lm,2}$ (black squares).

The effective diffusivity of each layer has been determined as:

$$D_e = D\frac{\varepsilon}{\tau} \tag{14}$$

where D is the water vapor diffusivity through the porous medium, taken as 0.388 $cm^2\ s^{-1}$; ε is the porosity; τ is the tortuosity, evaluated from the models of Mackie and Mears, Wackao and Smith, Suzuki and Smith. Knudsen diffusion effect has been also considered for MPL [24]. Being the two layers connected in series, total diffusivity has been calculated as:

$$D_{e,tot} = \frac{t}{(t_{MPL}/D_{e,MPL}) + (t_{GDL}/D_{e,GDL})} \tag{15}$$

where $t = t_{MPL} + t_{GDL}$ is total thickness.

Hence the water transfer coefficient, neglecting the contribution of advection, results:

$$K = \frac{D_e}{t} = \left(\frac{t_{MPL}}{D_{e,MPL}} + \frac{t_{GDL}}{D_{e,GDL}}\right)^{-1} \tag{16}$$

Based on the quantities listed in Table 2, K for GDL with MPL is found to vary within 0.7 and 3.7 cm s^{-1}. Apart from the strong variability of the model results, the measured data lie in the predicted range. Moreover, the model that considers the contribution of Knudsen diffusion seems to reproduce more accurately experimental data.

The effect of MPL can be highlighted in considering the measurements relative to SGL10AC, similar to SGL10CC without micro-porous layer. The results of the same testing procedure are summarized in Fig. 8, where the global water transfer coefficient is reported versus the flooding index. Data for the SGL10CC, discussed above, are also reported for comparison. Three main differences stand out. At first, water transport through the GDL noticeably increases: actually, K is about three times higher than for the structure without micro-porous layer. These results are also in agreement with model estimations reported in Table 2. Secondly, the decrease of the global water transfer coefficient for $FC > 1$ is more evident: as an example, for $FC = 1.5$, K shows 35% maximum relative reduction without MPL against 20% with MPL. Thirdly, it is to be noted that data are affected by greater variance.

In summary, the MPL seems to provide a reduction of flooding effect and a better stability of water transport, although reducing the mass transfer rate through the GDL. These observations are coherent with the results of several experimental analyses reported in literature [3,17–22] that evaluate GDL influence directly on PEMFC performance.

Moreover these results agree with the argumentations reported in [4,5]: saturated water concentration is higher inside the MPL than inside the GDL, due to smaller pore size and enhanced hydrophobicity, making the MPL less subject to flooding and less sensitive to its effect.

Table 2
Properties estimation for GDL and MPL, considering for the latter the possible contribution of Knudsen diffusivity.

	Thickness (μm)	Pore diameter (μm)	Porosity	Tortuosity	K (cm s^{-1})
GDL	350	10–30	0.6–0.8	1.8–3.3	2–5
MPL	50	0.1–0.5	0.4–0.6	3.3–6.4	5–14
MPL (Knudsen)	50	0.1–0.5	0.4–0.6	3.3–6.4	1–2.5
GDL + MPL	400	–	–	–	1.4–3.7
GDL + MPL (Knudsen)	400	–	–	–	0.7–1.7

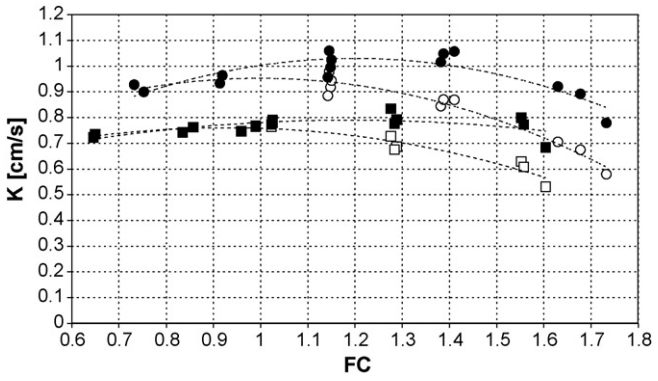

Fig. 9. Global water transfer coefficient versus flooding index for SGL10CC (squares) and ELAT LT1400W (circles), considering ΔC_{lm} (white) and $\Delta C_{lm,2}$ (black).

GDL and MPL are confirmed to have crucial roles in water management, thus their properties and structures should be accurately designed to minimize flooding and membrane dehydration effects.

Finally, data for an ELAT GDL are reported in Fig. 9, where they are compared with the reference SGL. The behaviors are quite similar, apart from a greater value of K for ELAT that could enhance water and oxygen transport and probably fuel cell performance.

4. Conclusion

This work presented a methodology to perform quantitative characterization of water transfer across a GDL in real operating conditions and the results of its application to some commercial components. The following conclusions can be drawn:

- the proposed methodology results accurate, reliable and reproducible;
- flooding onset and its effect on water transport were characterized for different GDL; the results are coherent with literature;
- typical values and range of variation of a global water transport coefficient through GDL have been determined and a quantitative index to establish the onset of flooding has been defined;
- MPL seems to provide a reduction of flooding effect and a better stability of water transport, although reducing the mass transfer rate through the GDL; water transport coefficient in flooding condition shows 35% maximum relative reduction without MPL against 20% with MPL;
- GDL and MPL are confirmed to have crucial roles in water management, thus their properties and structures should be carefully designed to minimize flooding and membrane dehydration effects.

Acknowledgment

Funding for this work from Fondazione Cariplo under agreement n. 2007.5543 is acknowledged.

References

[1] F.A. de Bruijn, V.A.T. Dam, G.J.M. Janssen, Fuel Cells 08 (1) (2008) 3–22.
[2] N. Yousfi-Steinera, P. Mocoteguya, D. Candusso, J. Power Sources 183 (2008) 260–274.
[3] S. Li, Y. Tang, Z. Wang, et al., J. Power Sources 178 (2008) 103–117.
[4] N. Holmstrom, J. Ihonen, A. Lundblad, G. Lindbergh, Fuel Cells 7 (2007) 306.
[5] D. Spernjak, A.K. Prasad, S.G. Advani, J. Power Sources 170 (2007) 334.
[6] U. Pasaogullari, C.Y. Wang, K.S. Chen, J. Electrochem. Soc. 152 (2005) A1574–A1582.
[7] F.Y. Zhang, X.G. Yang, C.Y. Wang, J. Electrochem. Soc. 153 (2006) A225–A232.
[8] R. Satija, D.L. Jacobson, M. Arif, S.A. Werner, J. Power Sources 129 (2004) 238.
[9] S. Tsushima, T. Nanjo, K. Nishida, S. Hirai, ECS Trans. 1 (2006) 199.
[10] P.K. Sinha, P. Halleck, C. Wang, Electrochem. Solid-State Lett. 9 (2006) A344–A348.
[11] A. Bazylak, D. Sinton, Z.-S. Liu, N. Djilali, J. Power Sources 163 (2007) 784–792.
[12] J. Chen, T. Matsuura, M. Hori, J. Power Sources 131 (2004) 155–161.
[13] E.C. Kumbur, K.V. Sharp, M.M. Mench, J. Power Sources 161 (2006) 333–345.
[14] H. Dohle, R. Jung, N. Kimiaie, J. Mergel, M. Muller, J. Power Sources 124 (2003) 371–384.
[15] A. Hakenjos, H. Muenter, U. Wittstadt, C. Hebling, J. Power Sources 131 (2004) 213.
[16] F. Barbir, H. Gorgun, X. Wang, J. Power Sources 141 (2005) 96.
[17] C. Lim, C.Y. Wang, Electrochim. Acta 49 (2004) 4149–4156.
[18] L.R. Jordan, A.K. Shukla, T. Behrsing, et al., J. Power Sources 86 (2000) 250–254.
[19] C. Quick, D. Ritzinger, W. Lenhert, C. Hartnig, J. Power Sources (2008) 110–120.
[20] J. Benziger, T. Whitaker, E. Kimball, I.G. Kevrekidis, ECS Trans. 12 (1) (2008) 67–79.
[21] S. Shimpalee, U. Beuscher, J.W. Van Zee, Electrochim. Acta 52 (2007) 6748–6754.
[22] S. Park, J.W. Lee, B.N. Popov, J. Power Sources 177 (2008) 457–463.
[23] 19 ISO, 1993. Guide to expression of uncertainty in measurement, BIPM, IEC, IFCC, ISO, IUPAC, IUPAP, OIML International organization for standardization, Env. 13005: 1999. led., corrected and reprinted 1995.
[24] R.H. Perry, D.W. Green, Perry's Chemical Engineer's Handbook, Mcgraw-Hill, 1999.